



PERGAMON

Solid State Communications 125 (2003) 317–322

solid
state
communicationswww.elsevier.com/locate/ssc

Extended X-ray absorption fine-structure (EXAFS) of a complex oxide structure: a full multiple scattering analysis of the Au L₃-edge EXAFS of Au₂O₃

N. Weiher^a, E.A. Willneff^{a,d}, C. Figulla-Kroschel^b, M. Jansen^c, S.L.M. Schroeder^{a,d,e,*}^a*Institut für Chemie, Freie Universität Berlin, Takustr. 3, 14195 Berlin, Germany*^b*Institut für Anorganische Chemie, Universität Bonn, Gerhard-Domagk-Str. 1, 53121 Bonn, Germany*^c*Max-Planck-Institut für Festkörperforschung, Heisenbergstraße 1, 70569 Stuttgart, Germany*^d*Molecular Materials Centre, Department of Chemical Engineering, P.O. Box 88, UMIST, Manchester M60 1QD, UK*^e*Department of Chemistry, P.O. Box 88, UMIST, Manchester M60 1QD, UK*

Received 13 October 2002; accepted 28 November 2002 by C.N.R. Rao

Abstract

Crystalline Au₂O₃ was obtained by hydrothermal synthesis at 3000 atm and its extended X-ray absorption fine-structure (EXAFS) at the Au L₃-edge was measured at room temperature. A detailed full multiple scattering (MS) analysis using FEFF8 theory shows that only a small number of scattering paths contribute significantly to the EXAFS of Au₂O₃. Because of the complex unit cell (low local symmetry) of the Au₂O₃ structure, contributions of MS paths are almost negligible. The results indicate that FEFF8 theory provides a good reference for the analysis of Au–O phases.

© 2003 Elsevier Science Ltd. All rights reserved.

PACS: 61.10.Ht; 61.10.Nz; 61.14.Dc; 61.66.Fn

Keywords: A. Insulators; A. Chemical synthesis; C. EXAFS, NEXAFS, SEXAFS; E. Synchrotron radiation; E. X-ray and γ -ray spectroscopies

1. Introduction

Phases in the binary system oxygen–gold have recently attracted much attention because they are intermediates in the preparation and operation of heterogeneous oxidation catalysts that contain small gold particles in contact with a support material [1–3]. Improvements to catalytic technologies require insight into the structural and electronic properties of these elusive and non-stoichiometric gold–oxygen compounds. Because of their low concentrations and strong crystallographic disorder this information is difficult to obtain with common structural probes based on the diffraction of X-rays or high-energy electrons. Extended X-ray absorption fine-structure (EXAFS) spectroscopy is

the foremost technique for elucidating the local structure of disordered phases under reaction conditions, but to date only few results on Au-based catalysts have been reported in the literature [4–7].

The determination of reliable structural information from EXAFS data requires reference parameters (phase shifts, scattering amplitudes, scattering angles) for the low-energy electron scattering events that are the origin of the EXAFS. Traditionally, these parameters have been obtained from EXAFS data of reference compounds with known structural parameters [8]. For condensed Au–O phases this route cannot be followed because well-defined reference compounds are not readily available. An alternative is the use of a theoretical reference spectrum, as, e.g. accessible with *ab initio* codes such as FEFF [9]. However, despite much progress in electron scattering theory [10] there remains some uncertainty whether the theoretical simplifications involved in calculating the scattering parameters are good approximations. A check against experimental data of

* Corresponding author. Address: Departments of Chemical Engineering and Chemistry, UMIST, P.O. Box 88, Manchester M60 1QD, UK. Tel.: +44-161-200-4502; fax: +44-161-200-4399.

E-mail address: s.schroeder@umist.ac.uk (S.L.M. Schroeder).

a reference compound is therefore advisable [10], especially for X-ray absorption edges of elements in the fifth and higher periods such as Au, where the core potential is so strong that relativistic contributions to the electronic structure of the atoms must be taken into account [11].

Currently, Au_2O_3 is the only stoichiometric binary compound of gold and oxygen with known crystallography and sufficient stability under ambient conditions [12,13]. Au_2O_3 is composed of a network of identical AuO_4 -units that contain two types of oxygen atoms in crystallographically distinct sites [15]: one oxygen atom is always shared between two AuO_4 -units, whereas each of the remaining three oxygen atoms connects to altogether three AuO_4 -units (see Fig. 4). The Au–O bond of the first type of oxygen atoms is slightly shorter (1.93 Å) than the other three Au–O bonds (2.01, 2.04, 2.07 Å). There are also out-of-plane distortion angles (in all cases less than 8°) between the four Au–O bonds, leading to additional deviations from an ideal square planar symmetry.

Unfortunately, the synthesis of stoichiometric Au_2O_3 is laborious: it involves hydrothermal conditions with pressures of several 1000 atm [14–16], which require safety precautions met in only few laboratories (we have found that ‘ Au_2O_3 ’ offered by several suppliers of chemicals is a strongly disordered, hydrated material). The difficulties in obtaining the compound are reflected by a scarcity of physical data reported in the literature. There have been only a powder [16] and a single crystal X-ray diffraction (XRD) study [14,15], some thermochemical measurements [17,18], and an X-ray absorption near-edge structure (XANES) investigation [19] elucidating the Au d-band occupancy in comparison with other gold compounds.

To provide other researchers with a standard for future EXAFS characterization of Au–O phases we report here the Au L_3 -edge EXAFS of crystalline Au_2O_3 . We discuss the results of a full multiple scattering (MS) analysis by means of the FEFF8 code [9], which shows that FEFF8 provides a meaningful theoretical reference for the analysis of Au–O compounds.

2. Experimental

Samples of crystalline Au_2O_3 were prepared by hydrothermal synthesis as described previously [18]. Briefly, a pressure of 3000 bar and a temperature of 600 K was applied to a 1 M solution of HAuCl_4 for 6 weeks. This treatment resulted in a mixture of crystalline Au_2O_3 and metallic Au. A powder diffraction analysis of the sample indicated that it contained approximately 80 mol% Au_2O_3 and 20 mol% Au, both as well-ordered phases (Fig. 1). A line-width analysis of the XRD pattern using the Scherrer formula [20] indicated that the average crystallite size of Au_2O_3 was at least ≈ 20 nm in every crystallographic direction. The line-

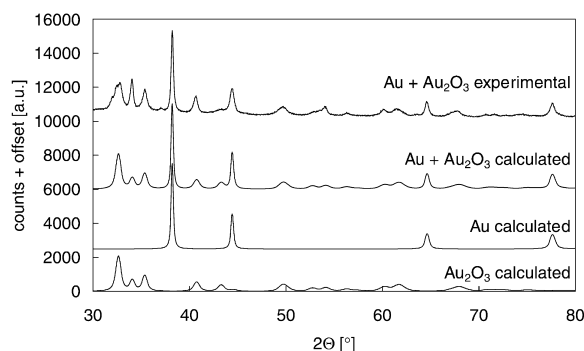


Fig. 1. XRD pattern of the sample used for the EXAFS acquisition. The upper pattern is the experimental pattern. A simulation by PowderCell [25] yielded the patterns below for a physical mixture containing 80% Au_2O_3 and 20% Au.

widths of the diffraction lines are unevenly distributed across the diffraction pattern (note especially the more narrow lines at 34.25° and 54.23°), which is evidence for growth of the Au_2O_3 crystallites in a preferred direction (e.g. through a needle-like shape of the crystallites, Fig. 1).

Au L_3 -edge EXAFS spectra were measured at the X1 beamline of HASYLAB (Hamburg, Germany). Throughout the XAS measurements, the double-crystal Si(311) monochromator was kept detuned at 60% of maximum reflectivity to suppress harmonics in the X-ray beam. The sample was carefully diluted in boron nitride and the thickness of this mixture adjusted in the sample holder until an absorption edge step of 1.2 was obtained at the Au L_3 -edge. A 5 μm thick Au foil (99.999%) was used as a standard sample. The intensity of the incoming and the transmitted beam was monitored with ion chambers filled with pure nitrogen and pure argon, respectively. During

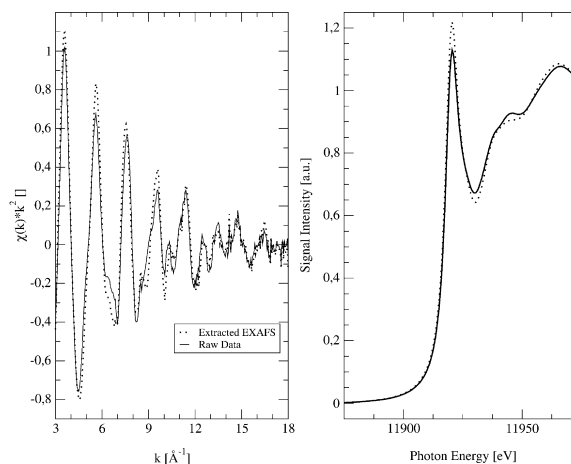


Fig. 2. Au L_3 X-ray absorption edge spectrum of Au_2O_3 ; left: EXAFS region, right: XANES region. The full lines represent the raw spectrum of the hydrothermally prepared sample. The dotted lines represent the spectrum obtained after subtracting the contribution of metallic Au as described in the text.

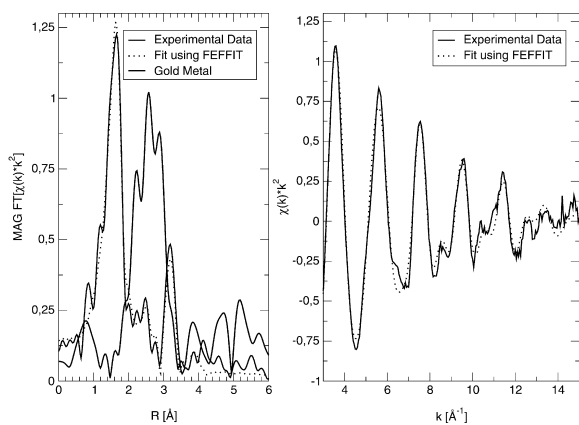


Fig. 3. Results of the EXAFS analysis of Au_2O_3 ; left: Fourier-transformed EXAFS, in comparison with the EXAFS spectrum of metallic Au (light grey); right: experimental EXAFS (full line) vs. the calculated fit as described in the text (dotted line). The fit parameters are summarised in Table 3.

measurements, the synchrotron storage ring operated in multi-bunch mode, with ring currents between 60 and 80 mA. Data acquisition times for one spectrum were about 30 min.

Data analysis was performed using the MS code FEFF8 to calculate theoretical scattering parameters [9]. Atomic positions for the cluster calculation of atomic potentials in Au_2O_3 were obtained from structural data provided in Ref. [14]. AUTOBK [21] was used to subtract the atomic background functions from the raw absorption spectra and to calculate the EXAFS by normalisation to the absorption edge step height. The contributions of scattering paths were determined with FEFFIT [22].

3. Results and discussion

The Au L_3 -edge spectrum of the hydrothermally prepared sample is presented in Fig. 2. To identify the

contribution of Au metal to the EXAFS of the Au_2O_3 sample we analysed the intensity of the single scattering paths of the nearest neighbour atoms in the oxide (four O atoms at approximately 2.00 Å) and in Au metal (12 Au atoms at 2.92 Å). This simple procedure is expected to provide a reliable analysis of the phase composition because Fourier filtering separates the near-neighbour scattering contributions of both phases from all other scattering paths. The separation is clearly seen in Fig. 3, which contains the Fourier-transformed EXAFS spectra of the Au foil and of Au_2O_3 . The near-neighbour EXAFS contributions were thus extracted by applying a Fourier window with Hanning boundaries at 1 and 3 Å.

The results of this phase analysis are given in Table 1. The fraction of Au_2O_3 contributions was found to be 84 ± 4 at.%, which is in very good agreement with the result of the XRD analysis. The good match between phase analyses obtained with a long-range (XRD) and a short-range (EXAFS) probe also indicates that XRD-invisible ('amorphous') components in the sample were at most a few at.%.

Contributions of metallic Au to the absorption spectrum of Au_2O_3 were removed by taking the edge-step-normalised absorption spectrum of the Au foil reference, scaling it by the weighting factor obtained from the phase analysis (i.e. 0.16), and subtracting it from the spectrum of the Au_2O_3 sample. In Fig. 2, the resulting Au_2O_3 near-edge spectrum (re-normalised to its edge-step height) and its EXAFS are compared to the parent spectrum of the mixture. The significant differences in the near-edge (XANES) and EXAFS regions of the raw and processed data are evident.

The Au L_3 -edge EXAFS of Au_2O_3 was analysed as follows. Using the path evaluation module of FEFF8 the significance of all theoretically possible scattering paths around a Au atom at the centre of a spherical Au_2O_3 cluster with a radius of 10 Å was examined. Among the 50 shortest scattering paths 43 paths were identified that had EXAFS amplitudes higher than 2.5% of the most intense path (which derives from backscattering at the most tightly bound, nearest oxygen atom at a distance of 1.93 Å). The results are

Table 1
Parameters obtained for Au/ Au_2O_3 sample composition analysis from first neighbour single scattering EXAFS

Parameter	Value	Statistical uncertainty
Fermi energy shift for gold metal (ΔE_{Au}) (eV)	-5	5
Fermi energy shift for gold oxide (ΔE_{O}) (eV)	17	2
First shell Debye–Waller factor for gold metal (σ_{Au}^2)	0.006	0.001
First shell Debye–Waller factor for gold oxide (σ_{O}^2)	0.030	0.005
First shell distance for gold metal as deviation from expected value (ΔR_{Au}) (Å)	-0.019	0.005
First shell distance for gold oxide as deviation from expected value (ΔR_{O}) (Å)	0.040	0.003
Fraction of Au atoms present as gold(III) oxide (%)	84	4

Independent points: 15; number of variables in fit: 7; remaining statistical degrees of freedom: 8; R -factor: 0.021; χ^2 : 294; reduced χ^2 : 36; k -space interval: [3:18]; R -space interval: [1:3].

Table 2
The 50 shortest scattering paths amplitudes higher than 2.5% (relative to #1) in Au₂O₃

#	Degeneracy	Length (Å)	Amplitude	Significant?	Atoms	Type
1	1	1.929	100.00	Y	Au–O–Au	Single
2	1	2.012	90.93	Y	Au–O–Au	Single
3	1	2.042	87.92	Y	Au–O–Au	Single
4	1	2.071	85.08	Y	Au–O–Au	Single
5	1	2.814	39.50	Y	Au–O–Au	Single
6	1	2.904	36.29	Y	Au–O–Au	Single
7	1	3.033	38.72	Y ^a	Au–Au–Au	Single
8	1	3.049	31.72	Y ^a	Au–O–Au	Single
9	1	3.193	27.86	Y	Au–O–Au	Single
10	2	3.337	64.14	Y ^a	Au–Au–Au	Single
11	2	3.351	63.55	Y ^a	Au–Au–Au	Single
12	2	3.352	11.44	N	Au–O–O–Au	Multiple
13	2	3.355	12.09	N	Au–O–O–Au	Multiple
14	2	3.446	3.79	N	Au–Au–O–Au	Multiple
15	2	3.459	59.40	Y	Au–Au–Au	Single
16	2	3.481	10.34	N	Au–O–O–Au	Multiple
17	2	3.559	10.22	N	Au–O–O–Au	Multiple
18	2	3.703	4.27	N	Au–Au–O–Au	Multiple
19	2	3.703	4.36	N	Au–Au–O–Au	Multiple
20	2	3.710	3.81	N	Au–Au–O–Au	Multiple
21	2	3.710	3.95	N	Au–Au–O–Au	Multiple
22	2	3.787	4.41	N	Au–Au–O–Au	Multiple
23	2	3.787	4.50	N	Au–Au–O–Au	Multiple
24	2	3.838	46.88	Y	Au–Au–Au	Single
25	1	3.858	8.12	N	Au–O–Au–O–Au	Multiple
26	1	3.892	15.50	N	Au–O–Au	Single
27	1	3.894	15.47	N	Au–O–Au	Single
28	1	3.911	15.27	N	Au–O–Au	Single
29	1	3.973	14.54	N	Au–O–Au	Single
30	2	3.997	21.15	Y ^b	Au–O–O–Au	Multiple
31	2	4.001	50.34	Y ^a	Au–O–Au–O–Au	Multiple
32	1	4.025	6.69	N	Au–O–Au–O–Au	Multiple
33	2	4.053	20.18	Y ^b	Au–O–O–Au	Multiple
34	2	4.055	48.27	Y ^a	Au–O–Au–O–Au	Multiple
37	1	4.084	6.25	N	Au–O–Au–O–Au	Multiple
43	1	4.143	5.85	N	Au–O–Au–O–Au	Multiple
44	1	4.248	11.76	N	Au–O–Au	Single
45	2	4.304	4.27	N	Au–O–O–Au	Multiple
46	2	4.312	35.10	N	Au–Au–Au	Single
47	1	4.331	11.06	N	Au–O–Au	Single
48	2	4.397	33.38	N	Au–Au–Au	Single
49	2	4.407	3.44	N	Au–O–O–Au	Multiple
50	2	4.421	2.71	N	Au–O–O–Au	Multiple

^a Included in the analysis as linear combinations.

^b Scattering path practically identical to the next path in the table, therefore not included separately.

summarised in Table 2: up to path lengths of approximately 4 Å the EXAFS is dominated by single scattering events. For distances around 4 Å, MS paths with an intensity of more than approximately 10% of the strongest scattering path are predicted: first, there are the scattering paths #30 (intensity: 21%) and #31 (intensity: 50%). They are almost identical, both starting with scattering at the nearest oxygen atom (labelled '1' in Fig. 4). Path #30 then proceeds directly to the oxygen atom opposite in the AuO₄-unit (labelled '4'

in Fig. 4) before returning back to the central Au atom. Formally, it is therefore a triangular scattering path, but it bypasses the central Au atom on its second leg so closely that the electron wave is significantly influenced by the atomic potential. As a result, this path is almost identical with the triple scattering path #31, which passes to the opposite oxygen atom *through* the central Au atom (rather than bypassing it), i.e. in three almost collinear scattering events. Collinear MS is well known to be an efficient

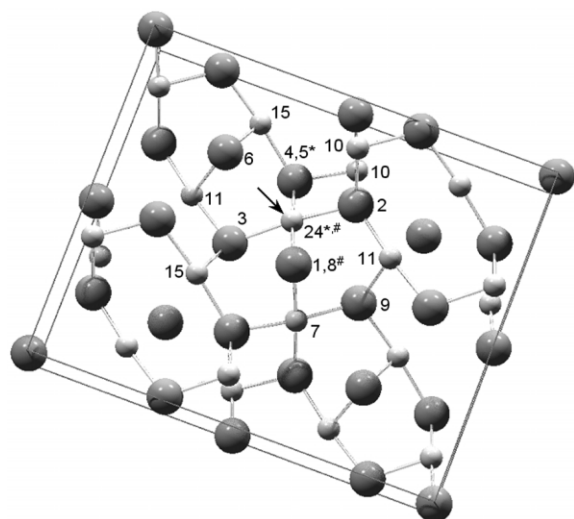


Fig. 4. The Au_2O_3 unit cell viewed along the c -axis, with all Au–O near-neighbour bonds drawn. Small, grey spheres represent Au atoms, whereas the larger, darker spheres depict oxygen atoms. Atoms included in the EXAFS analysis are numbered according to the corresponding single scattering paths in Table 2. The arrow marks the central Au atom. Note that some atoms are marked twice: asterisk indicates that the equivalent atom in the next unit cell *above* the drawing plane is responsible for the single scattering path. Similarly, a hash mark indicates scattering from the equivalent atom in the next unit cell *below* the plane. Note also that there are two inequivalent oxygen species in the structure, which are characterised by two (e.g. those marked as 1 and 6) and three (e.g. those marked as 2, 3 and 9) near-neighbour Au atoms (see the text).

scattering process (an important example is the scattering in the fcc- and rocksalt structures [24]), and explains the high intensity of the paths #31 and #30.

The other significant MS paths are #33 and #34: the origin of their high intensity is analogous to that of the paths #30 and #31 as they involve scattering at the other pair of opposite oxygen atoms in the AuO_4 -units (labelled ‘2’ and ‘3’ in Fig. 4). All other MS paths, including the ‘ping-pong’ double scattering path to the nearest neighbour (path #25), have much lower relative intensities, which never exceed approximately 12%. In contrast, no single scattering path with a length below 3.85 Å has amplitude of less than approximately 30%. The theoretical analysis of electron backscattering in Au_2O_3 thus predicts that an analysis of the experimental EXAFS based on single scattering paths (and possibly the two mentioned pairs of intense MS paths) with lengths up to approximately 4 Å should provide a good fit to the experimental spectrum. Indeed, the Fourier transform of the experimental EXAFS (Fig. 3) indicates that longer scattering paths contribute little, with a combined intensity corresponding to less than approximately 10% of the whole spectrum, so that they can be omitted from the analysis.

The results of our fitting analysis (Table 3) confirm these predictions. There is good agreement between calculation and experiment upon inclusion of all single scattering paths with lengths below 3.85 Å. It should be pointed out, however, that the lengths of the scattering pairs #7 and #8 as well as of #10 and #11 are too close to be resolved by the experimental EXAFS. Their scattering contributions were therefore taken into account as weighted linear combinations, using the weighting factor as a constraint in the analysis (the weighting factors are given in Table 3). Although adding the important multiple scattering pairs (#30/#31 and #33/#34) in the fitting procedure (as one

Table 3

Parameters obtained from the analysis of the Au L_3 EXAFS of Au_2O_3 . The scattering paths labelled ‘hybrid’ represent a linear combination defined by the additional weighting parameter given in the brackets

Atoms	Type	Weight	R (Å) ^a	ΔR (Å) ^b	DW-factor (σ^2)	Path degeneracy
Au–O	SS	–	1.929	0.075	0.004	4
Au–O	SS	–	2.814	0.095	0.013	2
Au–O	SS ^c	0.35	3.033	0.021 ^c	0.006 ^c	1
Au–Au	SS ^c	0.65	3.049			1
Au–O	SS	–	3.193	–0.031	0.003	1
Au–Au	SS ^c	0.48	3.337	0.027 ^c	0.006 ^c	1
Au–Au	SS ^c	0.52	3.351			1
Au–Au	SS	–	3.459	–0.031	0.009	2
Au–Au	SS	–	3.838	0.042	0.013	2
Au–O–Au–O	MS ^c	0.50	4.001	0.000 ^c	0.038 ^c	2
Au–O–Au–O	MS ^c	0.50	4.055			2

Overall amplitude factor S_0^2 : 0.82; Fermi-energy shift: 16.1 eV; independent points: 39.5; number of variables in fit: 23; remaining statistical degrees of freedom: 16.5; R -factor: 0.022; χ^2 : 1105; reduced χ^2 : 28; k -space interval: [3:18]; R -space interval: [1:5].

^a Distances as expected from crystal structure published in Ref. [14].

^b Deviation from expected distance.

^c Included in the analysis as weighted linear combinations (R included as weighted mean of the expected distances).

unified path) improved agreement between calculated and experimental data somewhat, all other MS paths turned out to be insignificant.

The strong dominance of single scattering contributions to the EXAFS is unusual for a binary oxide. It reflects the fact that the relatively open and complicated network structure of the covalent oxide Au_2O_3 results in a low local symmetry around the Au absorbers. As a result, there are no MS paths with high degeneracy levels as, e.g. in cubic oxides with the rock salt structure [24]. The values obtained for the Debye–Waller factors (σ^2) are for all paths within reasonable limits. In line with the good crystallinity of the sample use of the cumulant expansion [23] for the contributions of disorder did not improve the fit quality significantly. Another indication for insignificant disorder levels is the value of 0.82 for the overall amplitude factor S_0^2 , which is, within error limits, comparable to values obtained for other crystalline systems.

In summary, we have reported the first EXAFS analysis of a crystalline Au–O compound, which provides a reference for future studies of Au–O systems. The low local coordination symmetry around the AuO_4 -units in Au_2O_3 is associated with a large number of distinct single scattering paths, which dominate the EXAFS. The good agreement between the predictions of FEFF8 theory and the fitting analysis of the experimental data indicates that FEFF8 provides a good theoretical standard for the analysis of electron scattering in Au–O phases.

Acknowledgements

We thank the Fonds der Chemischen Industrie (FCI) for financial support for NW through a *Fondsstipendium*. We are grateful to HASYLAB for the provision of beamtime under Project No. II-99-025. This work was financially supported by Deutsche Forschungsgemeinschaft (DFG) under contract No. SCHR677/2-1.

References

- [1] G.C. Bond, D. Thompson, Catal. Rev.—Sci. Engng 41 (1999) 319.
- [2] G.C. Bond, D.T. Thompson, Gold Bull. 33 (2000) 41.
- [3] M. Haruta, Gold Bull. 34 (2001) 40.
- [4] H. Kageyama, et al., Jpn. J. Appl. Phys. 32 (2) (1993) 445.
- [5] I.W. Bassi, et al., J. Catal. 42 (1976) 139.
- [6] G. Cocco, et al., J. Phys. Chem. 83 (1979) 2527.
- [7] A. Balerna, et al., Surf. Sci. 156 (1985) 206.
- [8] D.E. Sayers, B.A. Bunker, in: D.C. Koningsberger, R. Prins (Eds.), X-ray Absorption: Principles, Applications, Techniques of EXAFS, SEXAFS and XANES, Chemical Analysis, vol. 92, Wiley, New York, 1988, p. 211.
- [9] A.L. Ankudinov, et al., Phys. Rev. B 58 (1998) 7565.
- [10] J.J. Rehr, R.C. Albers, Rev. Mod. Phys. 72 (2000) 621.
- [11] N. Bartlett, Gold Bull. 31 (1998) 22.
- [12] M. Jansen, A.V. Mudring, in: H. Schmidbaur (Ed.), Gold: Progress in Chemistry, Biochemistry and Technology, Wiley, Chichester, 1999.
- [13] Gmelin Handbook of Inorganic and Organometallic Chemistry. Au—Gold Supplement, vol. B1, Springer, Berlin, 1992, p. 59.
- [14] P.G. Jones, et al., Acta Crystallogr. B 35 (1979) 1435.
- [15] E. Schwarzmann, et al., Z. Naturforsch. 31b (1976) 135.
- [16] E. Schwarzmann, G. Gramann, Z. Naturforsch. 25b (1970) 1308.
- [17] E. Schwarzmann, E. Fellwock, Z. Naturforsch. 26b (1971) 1369.
- [18] S.J. Ashcroft, E. Schwarzmann, J. Chem. Soc., Faraday Trans. 1 68 (1972) 1360.
- [19] A. Pantelouris, et al., J. Am. Chem. Soc. 117 (1995) 11749.
- [20] H.P. Klug, L.E. Alexander, X-ray Diffraction Procedures: For Polycrystalline and Amorphous Materials, 2nd ed., Wiley, New York, 1974.
- [21] M. Newville, et al., Jpn. J. Appl. Phys. 32 (2) (1993) 125.
- [22] E.A. Stern, et al., Physica B 209 (1995) 117.
- [23] E.D. Crozier, et al., in: D.C. Koningsberger, R. Prins (Eds.), X-ray Absorption: Principles, Applications, Techniques of EXAFS, SEXAFS and XANES, Wiley/Interscience, New York, 1988, p. 373.
- [24] B. Lengeler, in: M. Campagna, R. Rosei (Eds.), Photoemission and Absorption Spectroscopy of Solids and Interfaces with Synchrotron Radiation, North-Holland, Amsterdam, 1990, p. 157.
- [25] W. Kraus, G. Nolze, Federal Institute for Materials Testing and Research (BAM), Rudower Chaussee 5, 12489 Berlin, Germany.